Nanostructure Stability and Swelling of Ternary Block Copolymer/Homopolymer Blends: A Direct Comparison Between Dissipative Particle Dynamics and Experiment

Amy D. Goodson,[1] **Guoliang Liu**,[2] **Maxwell S. Rick**,[1] **Andrew W. Raymond**,[1] **Md Fakar Uddin**,[1] **Henry S. Ashbaugh**,[1] **Julie N. L. Albert**[1]

[1]Department of Chemical and Biomolecular Engineering, Tulane University, New Orleans, Louisiana 70118
[2]Department of Chemistry and Macromolecules Innovation Institute, Virginia Tech, Blacksburg, Virginia 24061
Correspondence to: H. S. Ashbaugh (E-mail: hanka@tulane.edu); J. N. L. Albert (E-mail: jalbert6@tulane.edu)

Received 19 February 2019; revised 17 April 2019; accepted 17 April 2019; published online 29 April 2019
DOI: 10.1002/polb.24834

ABSTRACT: Ternary block copolymer (BCP)-homopolymer (HP) blends offer a simple method for tuning nanostructure sizes to meet application-specific demands. Comprehensive dissipative particle dynamic (DPD) simulations were performed to study the impact of polymer interactions, molecular weight, and HP volume fraction (φ_{HP}) on symmetric ternary blend morphological stability and domain spacing. DPD reproduces key features of the experimental phase diagram, including lamellar domain swelling with increasing φ_{HP}, the formation of an asymmetric bicontinuous microemulsion at a critical HP concentration φ^{*}_{HP}, and macrophase separation with further HP addition. Simulation results matched experimental values for φ^{*}_{HP} and lamellar swelling as a function of HP to BCP chain length ratio, $\alpha = N_{HP}/N_{BCP}$. Structural analysis of blends with fixed φ_{HP} but varying α confirmed that ternary blends follow the wet/dry brush model of domain swelling with the miscibility of HPs and BCPs depending on α. Longer HPs concentrate in the center of domains, boosting their swelling efficiencies compared to shorter chains. These results advance our understanding of BCP-HP blend phase behavior and demonstrate the value of DPD for studying polymeric blends. © 2019 Wiley Periodicals, Inc. J. Polym. Sci., Part B: Polym. Phys. **2019**, *57*, 794–803

KEYWORDS: blends; block copolymers; dissipative particle dynamics; simulation

INTRODUCTION Block copolymers (BCPs) consist of two or more chemically distinct homopolymers (HPs) covalently-bound into a single polymer. Monomer incompatibilities drive unlike blocks to minimize their contact, but the presence of the covalent bond prevents macroscopic phase separation so that BCPs self-assemble into a variety of nanoscale morphologies to minimize their frustration.[1,2] The ability to precisely control BCP domain sizes is critical for many applications, including advanced lithography,[3–6] nanoporous membranes,[7–12] and biological templating.[13,14] Pure BCP feature sizes are dictated by degree of polymerization (N_{BCP}), architecture, relative block sizes, and block incompatibilities as captured by the Flory–Huggins interaction parameter (χ). Swelling domains by adding HPs to form ternary BCP-HP blends (A-*b*-B/A/B) offers a simple, synthesis-free method for tuning feature dimensions to meet application-specific demands.[15–19] Added HPs can also act as plasticizers, decreasing the annealing time for blends to equilibrate while reducing the number of morphological and orientational defects.[5,20] If the HP has a low enough degree of polymerization (relative to the BCP), then these kinetic benefits can be realized with negligible impact on domain spacing. Exploiting BCP-HP blending to tune feature sizes requires a precise understanding of how polymer chemistry, degree of polymerization, and HP concentration impact phase behavior and morphological stability.

Experiments conducted over a wide range of polymer chemistries and molecular weights have established a general phase diagram for symmetric (equal volume fraction, $f_A = f_B = 0.5$) ternary blends.[6,15,16,20–23] For BCP segregation strengths (χN_{BCP}) above the order–disorder transition, pure symmetric BCPs form a lamellar structure. Blending in HPs while maintaining equal volume fractions of A and B components initially swells the lamellae, increasing domain sizes without changing morphology, until a critical homopolymer volume fraction (φ^{*}_{HP}), at which point the blend assumes a bicontinuous microemulsion (βμE) structure. The βμE displays local organization but is globally isotropic with zero mean curvature.[7] Following the βμE exists a second critical homopolymer concentration (φ^{**}_{HP}), after which the blend macroscopically separates into two distinct HP phases with the BCP acting as a compatibilizer at the interface. These morphological phase transitions have been studied as a function of χN_{BCP} and the ratio of the degree of polymerization of the HPs to that of BCP, $\alpha = N_{HP}/N_{BCP}$ with N_{HP} the same for both added HPs.[15] Experimentally, the lamellar-βμE

(φ^{*}_{HP}) and the βμE-macrophase (φ^{**}_{HP}) separation boundaries shift to lower HP volume fractions with increasing α, but are effectively independent of χN_{BCP}.[24]

Below φ^{*}_{HP}, HP addition swells the lamellae such that domain spacing (d) monotonically increases with φ_{HP}. The swelling efficiency of the homopolymer depends on its distribution within the block copolymer domains.[25] At one extreme, referred to as the "wet brush" regime, the HPs and matching BCP blocks are perfectly miscible so that HP chains are distributed evenly throughout the domain of the matching block. In this case, the lamellae are expected to swell isotropically with the domain spacing depending on φ_{HP} as[18,26]

$$d = \frac{d_0}{(1-\varphi_{HP})^{1/3}}, \quad (1)$$

where d_0 is the lamellar domain spacing of the pure BCP. At the other extreme, referred to as the "dry brush" regime, the HPs do not penetrate the BCP brush layers, instead segregating to the domain centers. In this case, the lamellae only swell in the direction normal to the lamellar plane as[18]

$$d = \frac{d_0}{1-\varphi_{HP}}. \quad (2)$$

Using an experimental ternary system of symmetric poly(styrene)-*b*-poly(methyl methacrylate) blended with equal amounts of constituent homopolymers (PS-*b*-PMMA/PS/PMMA), Liu et al. developed a phenomenological relationship of the same form as eqs 1 and 2. Specifically they proposed swollen domain spacings could be described as[15]

$$d = \frac{d_0}{(1-\varphi_{HP})^{\beta}} \quad (3)$$

where β is an empirically adjustable parameter. Theoretically, β should interpolate between 1/3 (eq 1) and 1 (eq 2). Experimentally, β was found to be a linearly increasing function of α, indicating longer HPs more strongly dewet the BCP brushes. Interestingly, Liu et al. reported the values of β greater than 1 for α values greater than 0.5 (where the HP degree of polymerization matches that of an individual BCP block), suggesting stretching of the HPs within a dewetted layer. We note that the blend BCPs are not technically polymer brushes because they are not tethered to a fixed interface but instead are able to move along the interface to accommodate the added HP. However, we refer to "brush wetting" and "brush dewetting" in ternary blends for consistency with previous literature[20,27–29] on the subject.

Even in the model symmetric ternary system, a multitude of different blends can be created by varying χ, N_{BCP}, α, and φ_{HP}. Molecular simulation allows for rapid exploration of blend combinations to optimize compositions that produce the desired morphologies and domain spacings, thereby shrinking the parameter space that must be examined experimentally. In this work, we use dissipative particle dynamic (DPD) simulations to complement the existing experimental results on symmetric ternary blends. DPD has been used extensively to model bulk BCP phase behavior since Groot and Madden first demonstrated in 1997 the ability of the technique to map BCP morphologies as a function of χN_{BCP} and f_A, the fractional A block volume.[30–34] DPD has also been shown to reproduce experimental morphology shifts in A-*b*-B/A[35] and A-*b*-B/C[36] binary BCP/HP blends. In contrast to mean field theories (MFTs), which neglect thermal fluctuations,[19,25,37–41] DPD simulations predict the formation of a βμE phase in symmetric ternary blends,[42] consistent with the experimental observation. We note that field theoretic simulations also find a βμE phase in ternary blends, but always in coexistence with A and B homopolymer phases.[39,43–45] Such three-phase systems have not been observed experimentally for $\alpha < 1$.

Here, we use DPD simulations to investigate the morphology and domain spacing of symmetric ternary blends as a function of HP content and relative chain length. By comparing our DPD results directly to experiments for PS-*b*-PMMA blended with PS and PMMA,[15] we show DPD more closely reproduces the experimental behavior than do mean field predictions. We then use our simulation results to explore the relationship between chain length, HP segregation, and swelling efficiency in ternary blends, showing that as α increases, the HP chains segregate more efficiently within each BCP domain.

METHODS

DPD Simulation Methodology

DPD simulations of BCPs were performed using the LAMMPS software package.[46] DPD is a coarse-grained simulation technique that groups many atomic sites together into a single effective bead with softer interbead interactions than atomically explicit methods. Each coarse-grained DPD bead represents tens of monomer units, allowing the simulations to reach sufficient time and length scales to study mesoscale BCP assembly. Significantly, DPD retains the inherent thermal fluctuations eliminated from MFTs that can be significant in polymer phase behavior.[30,47–49]

Interparticle forces in DPD are broken up into a sum of pairwise conservative ($\boldsymbol{F}^{C}_{ij}$), dissipative ($\boldsymbol{F}^{D}_{ij}$), and random ($\boldsymbol{F}^{R}_{ij}$) forces between particles i and j. Interactions between bonded particles are modeled using a Hookean spring ($\boldsymbol{F}^{S}_{ij}$), which enforces bead connectivity and polymer architecture. The net force on DPD bead i is subsequently determined as a sum over interactions with all other beads in the simulation[14,15]

$$\boldsymbol{F}_i = \sum_{j \neq i} \boldsymbol{F}^{C}_{ij} + \boldsymbol{F}^{D}_{ij} + \boldsymbol{F}^{R}_{ij} + \boldsymbol{F}^{S}_{ij}. \quad (4)$$

This force governs the time evolution of the particle system according to Newton's Laws of Motion; our simulations use the velocity Verlet algorithm[50] with a timestep Δt=0.025. The mass of each bead in the simulation is assumed to be m = 1.

The conservative (energy-conserving) force enforces the chemical identity of the constituent coarse-grained bead, modeled in DPD as a soft repulsive interaction

$$\boldsymbol{F}_{ij}^{C} = \begin{cases} \frac{a_{ij}}{r_c}\left(1-\frac{r_{ij}}{r_c}\right)\hat{\boldsymbol{r}}_{ij} & r_{ij} < r_c \\ 0 & r_{ij} \geq r_c \end{cases}, \quad (5)$$

where a_{ij} is the DPD interaction parameter between beads i and j (dependent on the chemical identities of the interacting beads) that represents the maximum repulsion at complete overlap, r_{ij} is the distance between interacting beads, $\hat{\boldsymbol{r}}_{ij} = \boldsymbol{r}_{ij}/r_{ij} = (\boldsymbol{r}_i - \boldsymbol{r}_j)/r_{ij}$ is the normalized direction vector pointing from j to i, and r_c is the cut-off distance after which interbead interactions vanish. For simplicity, we set $r_c = 1$ for all interbead interactions. The interaction between like beads, a_{AA} and $a_{BB,}$ which is set to 25, establishes the compressibility of the system while the interaction between unlike beads, a_{AB}, controls miscibility between the two blocks.[14] The value of a_{AB} chosen for this work ensured phase separation at low N_{DPD} and equilibration of simulations on reasonable time scales at high N_{DPD}. At a bead number density of $\rho = 3$ (the density of the simulations conducted here), the interbead interactions can be mapped to the Flory–Huggins χ parameter *via* the correlation[30]

$$\chi = \frac{1}{3.27}(a_{AB} - a_{AA}). \quad (6)$$

We note that as DPD is a coarse-grained simulation technique, we cannot directly compare simulation and experimental values of χ. Rather, DPD values of χ are typically calculated to match the experimental segregation strengths, that is, $\chi N_{BCP}|_{DPD} = \chi N_{BCP}|_{expt}$, to affect a meaningful comparison between simulation and experiment.[34] The simulations in this study were conducted with $a_{AB} = 65$ and $6 < N_{DPD} < 16$, which corresponds to a segregation strength range of $72 < \chi N_{BCP}|_{DPD} < 195$.

The dissipative force accounts for the viscous drag of the multiple atomic sites condensed onto a single coarse-grained bead. DPD models the dissipative force as

$$\boldsymbol{F}_{ij}^{D} = -\gamma \omega_{ij}^{D}(r_{ij})(\boldsymbol{v}_{ij}\cdot\boldsymbol{r}_{ij})\hat{\boldsymbol{r}}_{ij}, \quad (7)$$

where γ is the friction coefficient, and $\boldsymbol{v}_{ij} = \boldsymbol{v}_i - \boldsymbol{v}_j$ is the relative velocity between particles i and j. The random force accounts for thermal Brownian kicks from the coarsened degrees of freedom, modeled in DPD as

$$\mathbf{F}_{ij}^{R} = -\sigma \omega_{ij}^{R}(r_{ij})\frac{\zeta_{ij}}{\sqrt{\Delta t}}\hat{\boldsymbol{r}}_{ij}, \quad (8)$$

where σ is a constant noise amplitude related to the temperature, and ζ_{ij} is a Gaussian random number with a mean of zero and unit variance. The fluctuation dissipation theorem imposes the following constraints on the distance dependent weight functions $\omega_{ij}^{D}(r)$ and $\omega_{ij}^{R}(r)$ and the amplitudes of the viscous and random forces[51]:

$$\omega_{ij}^{D}(r_{ij}) = \left[\omega_{ij}^{R}(r_{ij})\right]^2 \quad (9a)$$

and

$$\sigma^2 = 2\gamma k_B T, \quad (9b)$$

where k_BT is the product of the Boltzmann's constant and the absolute temperature. Taken together then, eqs 7–9 act as a thermostat ensuring DPD simulations sample the canonical (constant NVT) ensemble. As the form of one of the weighting functions appearing in eqs 7 and 8 is arbitrary, for simplicity DPD simulations adopt the expression

$$\omega_{ij}^{D}(r_{ij}) = \left[\omega_{ij}^{R}(r_{ij})\right]^2 = \begin{cases} \left(1-\frac{r_{ij}}{r_c}\right)^2 & r_{ij} < r_c \\ 0 & r_{ij} \geq r_c \end{cases}, \quad (10)$$

which vanishes beyond r_c, like the conservative force. Here, we assume $k_BT = 1$ and $\sigma = 3$ ($\gamma = 4.5$) as recommended in Reference 47 to ensure fast, stable simulations.

Finally, the Hookean spring force in eq 4 is a second conservative interaction only between bonded beads that enforces intramolecular polymer connectivity. The spring force is evaluated as

$$F_{ij}^{S} = k r_{ij}\hat{\boldsymbol{r}}_{ij}, \quad (11)$$

where k is the spring constant, assumed here to be equal to 4,[30,48] independent of the chemical identity of the bonded monomers.

Canonical ensemble DPD simulations were performed of A_m-*b*-B_m BCPs blended with their constituent homopolymers (A_n and B_n) where the subscripts n and m denote the number of DPD beads in the respective polymer segments and thereby represent the degree of polymerization. In all cases, equal amounts of A_n and B_n HPs were added so that the blend retained the composition of the neat block copolymer. Homopolymer was added to the BCP in 10% increments to form blends that ranged from 0 to 80% homopolymer by volume. All blends consisted of 81,000 total beads in a periodic, cubic simulation box with side length $L = 30$, corresponding to a bead number density of $\rho = 3$. Simulations were started from random initial configurations and equilibrated for at least 10^6 timesteps. Following equilibration, production simulations were conducted for 5×10^5

TABLE 1 Summary of Ternary Blend Simulations Performed

N_{BCP}	N_{HP}	α
10	2	0.20
10	3	0.30
10	4	0.40
10	5	0.50
6	3	0.50
16	8	0.50
16	12	0.75
6	5	0.83
10	10	1.00

TABLE 2 Summary of Ternary PS-*b*-PMMA/PS/PMMA Blend Experiments Conducted[a]

$M_{PS-b-PMMA}/M_{PS}/M_{PMMA}$[b]	α
104/20.8/20	0.20
104/39/37	0.37
104/56.5/52	0.52
104/77/75	0.73
104/102.6/102.7	0.99

[a] These experiments were originally reported in Reference 15. As the lengths of the homopolymers cannot be precisely controlled, the ratio of the homopolymer to block copolymer chain lengths is determined by the geometric mean as $\alpha = \left[\left(\frac{M_{PS}}{F_{PS}}\right)\left(\frac{M_{PMMA}}{F_{PMMA}}\right)\right]^{\frac{1}{2}} / \left(\frac{M_{PS-b-PMMA}}{F_{PS-b-PMMA}}\right)$, where M_i and F_i are the number average molecular weight and mean monomer formula weight of polymer i. When $M_{PS}/F_{PS} = M_{PMMA}/F_{PMMA}$ the geometric mean calculation of α reduces to that evaluated from simulation.

[b] The molecular weights reported in this table are in kg/mol. The molecular weights of the PS and PMMA blocks of the polymer are 52 kg/mol a piece for a total molecular weight of 104 kg/mol. The formula weights of the PS and PMMA monomers are 104.1 and 100.1 g/mol, respectively.

timesteps. Structural quantities were calculated from configurations generated during the production run by averaging over a minimum of 50 configurations evenly sampled over the entire production run. All simulations were performed on the Ashbaugh group Dell cluster.

DPD results were compared with experimental ternary blends of roughly symmetric poly(styrene)-*b*-poly(methyl methacrylate) (PS-*b*-PMMA) with PS and PMMA homopolymers described in Reference 15. Note that domain spacings and morphology identifications of the experimental PS-*b*-PMMA/PS/PMMA blends are taken from Reference 15 but the images in Figure 2 from which these values were determined were not published previously. Due to the highly coarse-grained nature of DPD, comparisons were made between simulation and experiment based on $\alpha = N_{HP}/N_{BCP}$ (ratio of HP to BCP length), rather than absolute chain lengths (Tables 1 and 2).

Structural Analysis

Ordered nanostructures were initially identified visually by rendering the equilibrated simulation box using the program Visual Molecular Dynamics.[52] This visual identification was subsequently confirmed by evaluating the A monomer static structure factor

$$S_{AA}(q) = \frac{1}{n_A}\left\langle \left| \sum_{j=1}^{n_A} e^{i\boldsymbol{q}\cdot\boldsymbol{r}_{Aj}} \right|^2 \right\rangle, \quad (12)$$

where $\boldsymbol{r}_{Aj}$ is the position vector of A bead j, n_A is the total number of A beads, $\boldsymbol{q} = q_x\hat{\boldsymbol{i}} + q_y\hat{\boldsymbol{j}} + q_z\hat{\boldsymbol{k}}$ represents a wave vector,[32,53,54] and the angled brackets $\langle \ldots \rangle$ denote averaging over configurations and wave vector orientations. We note that due to the symmetry of the simulations $S_{AA}(q) = S_{BB}(q)$. Due to the cubic symmetry of the simulation box, the allowable wave vector set is $\{q_x, q_y, q_z\} = \{2\pi l/L, 2\pi m/L, 2\pi p/L\}$ where l, m, and p are integers from −15 to 15 excluding $\boldsymbol{q} = \boldsymbol{0}$. Our calculated

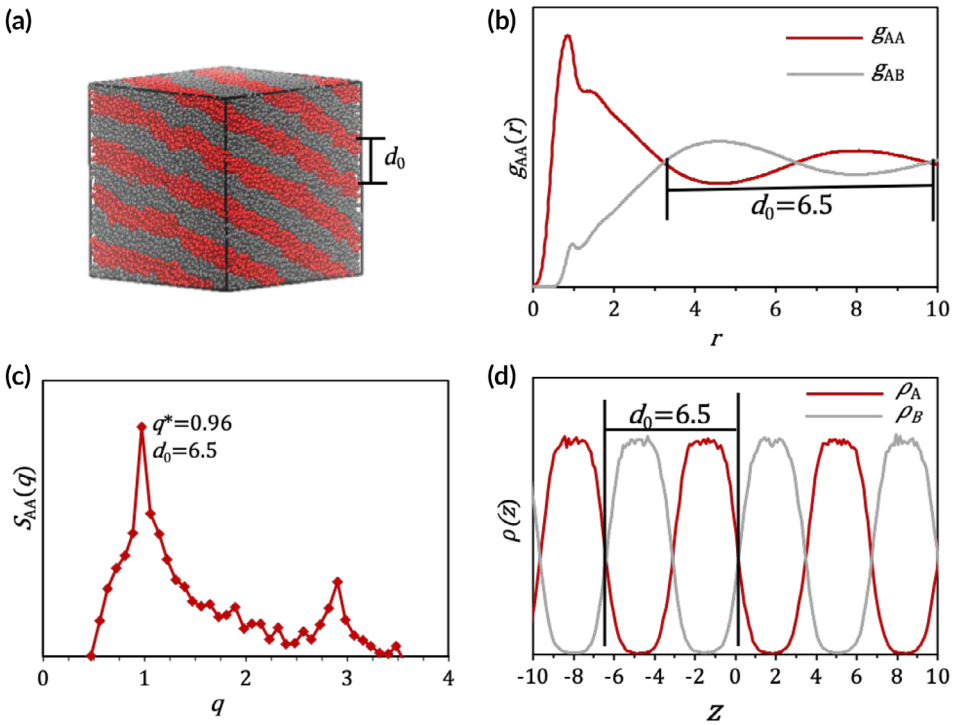

FIGURE 1 Calculation of domain spacing (d_0) for a pure A_5-*b*-B_5 BCP. The subscript 0 indicates the domain spacing of a pure BCP. (a) Snapshot of the equilibrated lamellar BCP. (b) In real space, d_0 is determined as the space between intersection points of $g(r)$ for like and unlike bead pairs. (c) In Fourier Space, d_0 is calculated from the primary scattering peak as $d = 2\pi/q^*$. (d) From density profiles, d_0 is readily calculated from the length of the repeat unit. [Color figure can be viewed at wileyonlinelibrary.com]

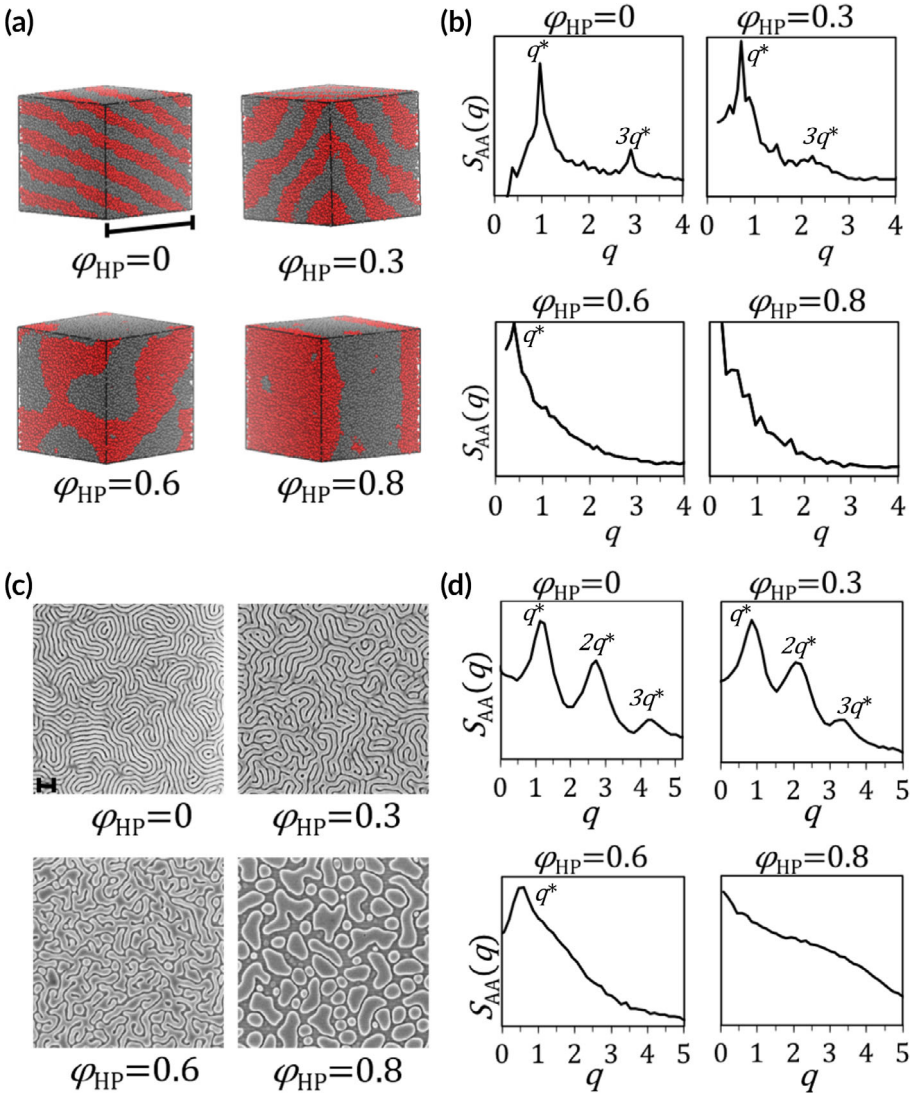

FIGURE 2 (a) Morphology snapshots and (b) static structure factors $S(q)$ of simulated A_5-*b*-$B_5/A_4/B_4$ ternary blends (α = 0.4) with increasing homopolymer content (φ_{HP}). The perfect symmetry of the DPD blends causes extinction of even-ordered peaks in the simulated $S(q)$. (c) Scanning electron microscopy (SEM) images and (d) static structure factors $S(q)$ (calculated by FFT of SEM images) of experimental PS-*b*-PMMA/PS/PMMA ternary blends with α = 0.37. In both experiment and simulation, the phase transition from lamellar to βμE occurs between φ_{HP} = 0.3 and 0.6 and the βμE to droplet microemulsion/two-phase transition occurs between φ_{HP} = 0.6 and 0.8. The scale bars in images (a) and (c) correspond to ~250 nm. [Color figure can be viewed at wileyonlinelibrary.com]

$S_{AA}(q)$ is proportional to the experimental X-ray scattering intensity and the fast Fourier transform (FFT) of real-space BCP images between $q = 2\pi/L \approx 0.2$ and $q = 2\pi/r_c \approx 6.3$. On the low end, the reliable q values are constrained by the simulation box length (L = 30), and at high q, we are limited by the approximate size of a DPD bead (r_c = 1). The polymer morphology is identified based on the ratio of the higher-order peaks relative to the primary peak at q^*.[26,55]

Domain spacings were calculated using the radial distribution functions between like and unlike beads, $g_{AA}(r)$ and $g_{AB}(r)$. Specifically, d is the distance between the first and third (or i and i + 2) crossing points between $g_{AA}(r)$ and $g_{AB}(r)$.[56] The radial distribution functions are related by Fourier transform to $S_{AA}(q)$ so d can also be calculated based on the location of the primary scattering peak as[26]

$$d = \frac{2\pi}{q^*}. \quad (13)$$

An alternate method for measuring lamellar domain spacings in simulation is to calculate density profiles of A and B beads along the direction normal to the lamellar interface. The distance between the first and third (or i and i + 2) crossing points of ρ_A and ρ_B gives the domain spacing. This density profile method provides an independent verification of the $g(r)$ calculations. Figure 1 demonstrates the use of $g_{AA}(r)$, $S_{AA}(q)$, and density profiles to

evaluate lamellar domain spacing in symmetric ternary blends. All methods give d spacings within 1% of each other.

RESULTS AND DISCUSSION

The impact of blending increasing amounts of homopolymer with a block copolymer ($\alpha \approx 0.4$) on melt morphology is illustrated in Figure 2. Qualitatively, simulations of ternary blends of A_5-b-$B_5/A_4/B_4$ show with increasing homopolymer volume fraction the lamellar polymer structure initially (up through φ_{HP} = 0.5) swells (i.e., the lamellar domain spacing increases) and develops increasing interfacial fluctuations as the homopolymer fluidizes the nanostructure, increasing the flexibility of the lamellar interface. By φ_{HP} = 0.6, the blend has formed a bicontinuous microemulsion (βμE) and at φ_{HP} = 0.8, it is phase-separated with BCP molecules at the interface (Fig. 2a). The scattering structure factors evaluated from our simulation configurations confirm this trend (Fig. 2b). For the lamellar domains ($\varphi_{HP} \leq 0.4$), the scattering intensity displays two peaks at q^* and $3q^*$. The expected peak at $2q^*$ for lamellae is not observed due to destructive interference from perfectly symmetric lamellar systems canceling out the even-ordered peaks.[55] In the case of the bicontinuous structure (φ_{HP} = 0.6), the structure factor exhibits only one peak associated with the correlation length of the blend.[7,23] For the phase separated blend, the scattering intensity increases with decreasing values of q, but a peak is not observed.

The trends observed in simulation mirror those determined experimentally. Scanning electron microscopy (SEM) images of perpendicularly oriented thin films of PS-b-PMMA/PS/PMMA ternary blends with α = 0.37 are shown in Figure 2c. For homopolymer volume fractions of φ_{HP} = 0 and 0.3, the SEM images display lamellar domains with spacings of ~50 nm. At φ_{HP} = 0.6, the lamellar order dissipates forming a βμE with no apparent long-range correlations between domains. At φ_{HP} = 0.8, the individual polymer domains have coalesced to form a phase that Reference 15 refers to as a "droplet microemulsion" as the length scale of macrophase separation is still on the micron length scale. However, in our simulations, this droplet microemulsion phase is indistinguishable from true macrophase separation due to simulation box size. The 2D-Fourier transform of these SEM images corroborates this assignment of polymer nanostructures (Fig. 2d). Specifically, the lamellar phases (φ_{HP} = 0 and 0.3) exhibit peaks in scattering intensity at q^*, $2q^*$, $3q^*$, and $4q^*$, while the βμE (φ_{HP} = 0.6) phase only exhibits a single scattering peak, and the droplet emulsion exhibits a single peak at exceptionally low q, well above the length scale we can probe with our simulations. The agreement between experiments and our simulations gives us confidence that DPD provides a realistic description of the phase behavior of ternary A_m-b-$B_m/A_n/B_n$ blends.

The relationship between homopolymer content, relative chain lengths, and ternary blend nanostructure is reported in Figure 3. Qualitatively, DPD simulation and experiments with PS-b-PMMA/PS/PMMA thin films both show the microemulsion channel gradually shifting to lower homopolymer content with increasing α, indicating that longer homopolymer chains more effectively disrupt the lamellar nanostructure. DPD predictions for both φ^*_{HP}, the homopolymer content at which the blend transitions from

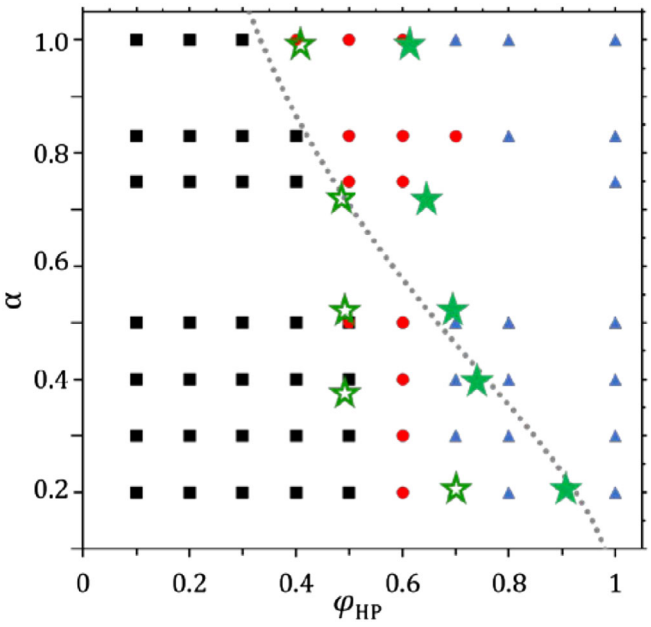

FIGURE 3 Morphologies observed in DPD simulations of A_m-b-$B_m/A_n/B_n$ blends as a function of φ_{HP} and α. Black squares, red circles, and blue triangles indicate lamellar, microemulsion, and two-phase microstructures, respectively. Empty and filled green stars indicate φ^*_{HP} and φ^{**}_{HP} observed in PS-b-PMMA/PS/PMMA blends,[15] respectively. The experimental phase transitions are shown halfway between the greatest φ_{HP} for which the lamellar (microemulsion) morphology was observed and smallest φ_{HP} that displayed a microemulsion (macrophase separated) morphology. The gray dotted line indicates the MFT prediction for the unbinding transition (eq 14).[38,57] [Color figure can be viewed at wileyonlinelibrary.com]

a lamellar structure to a βμE, and φ^{**}_{HP}, the blend composition at which macrophase separation occurs, track closely with experimental observations for $\alpha > 0.2$. The simulated φ^*_{HP} and φ^{**}_{HP} values begin to deviate from experiment for the shortest chain lengths simulated when $\alpha = 0.2$, corresponding to a blend of A_5-b-B_5 with A_2 and B_2 HPs. This discrepancy is due to the A and B "chains" becoming too short (2 DPD beads each) at small α to exhibit full polymeric behavior. Despite this discrepancy in the morphology transition, the $\alpha = 0.2$ case is still used in the study of domain swelling as the lamellar and BμE features follow the same domain spacing scaling with φ_{HP} (see Figures 4–6 and surrounding discussion), making the exact location of φ^*_{HP} irrelevant for that analysis.

MFT does not predict the existence of a microemulsion phase, instead finding that the lamellar period swells with increasing homopolymer content until it diverges at an unbinding transition determined by the analytical expression[38,57]

$$\varphi^*_{HP,UT} = \frac{1}{1+2\alpha^2} \text{ for } \alpha < 1. \quad (14)$$

According to MFT, ternary A_m-b-$B_m/A_n/B_n$ blends only exhibit a single critical homopolymer concentration at $\varphi^*_{HP,UT}$ after which

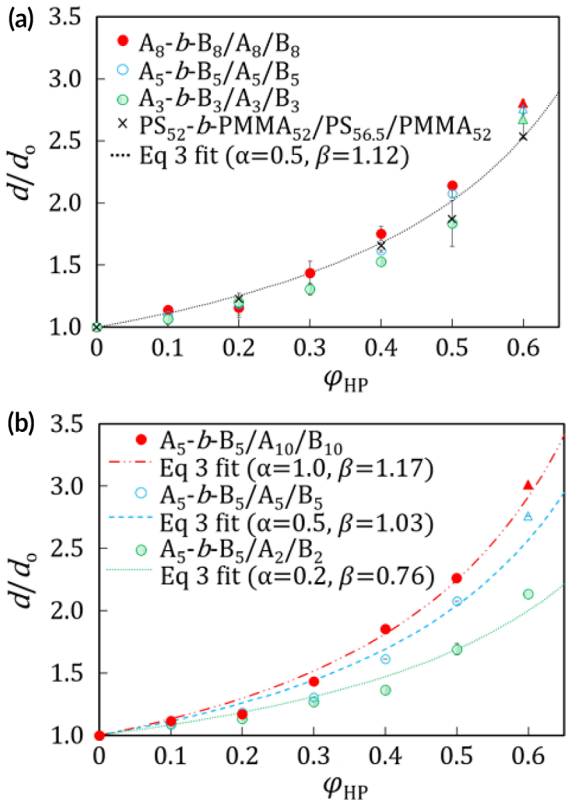

FIGURE 4 (a) Comparison of DPD simulation (A_n-b-$B_n/A_m/B_m$, colored circles) to experimental[15] (PS-b-PMMA/PS/PMMA, black crosses) swelling when $\alpha = 0.5$. The overlap of DPD data points for a given α value shows that swelling is controlled by the ratio of HP to BCP lengths, rather than the absolute chain lengths involved. (b) Lamellar swelling from DPD simulations (A_5-b-$B_5/A_m/B_m$, colored circles) demonstrates that swelling efficiency increases with α. Lines represent fits of simulation data to eq 3. In both figures, circles indicate lamellar morphologies and triangles represent the bicontinuous microemulsion. [Color figure can be viewed at wileyonlinelibrary.com]

the system undergoes macrophase separation. While eq 14 qualitatively captures the experimental and simulation shift in the stability boundary for the lamellar structures to higher concentrations with decreasing homopolymer length, MFT exaggerates the dependence of the critical concentration on α, overpredicting the lamellar stability as α tends toward 0 and underpredicting the lamellar stability as α tends toward 1. Comparatively, our DPD simulations provide a more accurate description of the experimental phase behavior. The reliability of DPD's predictions may be attributable to its inclusion of thermal fluctuations absent from MFT. This proposition is supported by experimental[23] and computational[42] results demonstrating that the bending modulus of the lamellar interface, κ, decreases with increasing homopolymer concentration, with the lamellar/microemulsion phase boundary occurring when $\kappa \sim k_B T$.

Having established the stability limits of the lamellar phase upon homopolymer addition, we now focus on the impact of HP addition on lamellar domain swelling for $\varphi_{HP} \le \varphi^*_{HP}$. The lamellar domain spacings of ternary A_m-b-$B_m/A_n/B_n$ blends as a function of φ_{HP} for $\alpha = n/(2m) = 0.5$ with m = 3, 5, and 8 are depicted in Figure 4a. As the HP concentration increases, our simulations find that d increases in a manner consistent with Liu et al.'s empirical model with an empirical swelling exponent of β = 1.12, which was calculated by fitting eq 3 to experimental measurements for PS-b-PMMA/PS/PMMA blends. While there is scatter in the simulation results, there is no clear trend between the results for different BCP lengths and the agreement between the data for the three different BCP lengths considered is quite good. This suggests the dominant contribution to the fractional extent of polymer swelling for fixed α is the HP concentration and not the absolute lengths of the constituent polymers, as postulated in the theoretical development above and consistent with previous experimental studies of ternary blends in the bulk and thin films.[15,21]

Figure 4b shows the dependence of domain spacing on homopolymer length in A_5-b-$B_5/A_m/B_m$ blends. Simulation results indicate that domain swelling increases with α for a given volume fraction of homopolymer in the blend; that is, longer homopolymers are more efficient at swelling BCP domains. We fit our simulation results to eq 3, calculating β for each set of simulations at a constant α value by least squares fit. We then plot the resultant models on Figure 4b to demonstrate that the eq 3 model is able to describe our swelling results in lamellar (circles) and bicontinuous microemulsion (triangles) morphologies.

We next compare our simulation swelling to experimental data by analyzing the relationship between α and β. Liu et al. found that β was a linear function of α, given as:

$$\beta(\alpha) = 1.067\alpha + 0.4767. \quad (15)$$

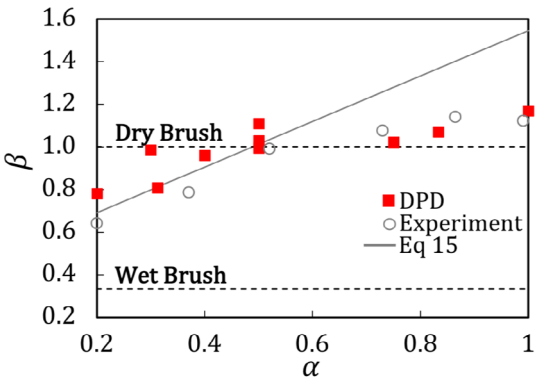

FIGURE 5 Comparison of β values calculated by fitting lamellar and bicontinuous phase domain spacings measured in DPD simulation (solid squares) and experiment (hollow circles) to eq 3. The solid line represents the original Liu et al. prediction (eq 15)[15] and the dashed lines give the wet (β = 1/3) and dry (β = 1) brush predictions. Both simulation and experiment show a flattening of the $\beta(\alpha)$ curve above β = 1 not captured by eq 15, suggesting that the dry brush conformation represents the maximum swelling attainable in a nanostructured ternary blend. [Color figure can be viewed at wileyonlinelibrary.com]

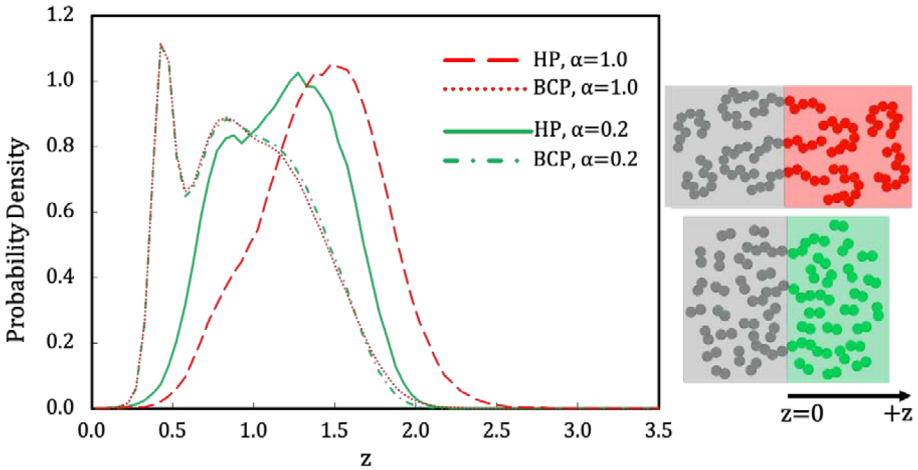

FIGURE 6 Probability density of observing BCP and HP monomers at a distance z from the A/B domain interface. The distance from the interface z is approximated by determining the minimum distance of a given monomer from the midpoint of the bond linking the A and B chains of any of the BCPs. Results are reported for BCPs of length $N = 10$ and $\alpha = 0.2$ and 1.0 with $\varphi_{HP} = 0.10$. The distributions for the A and B domains are equivalent due to the symmetry of the system. [Color figure can be viewed at wileyonlinelibrary.com]

This relationship came from fitting to eq 3 the domain spacings formed by PS-*b*-PMMA/PS/PMMA blends at constant α and φ_{HP} ranging from 0 (pure BCP) to 1 (pure HP). Calculating $\beta(\alpha)$ over this wide range of φ_{HP} meant that sizes of lamellar, bicontinuous microemulsion, droplet, and macrophase separated morphologies were all included in the fit. However, we are unable to obtain accurate domain spacings for droplet microemulsion and two-phase morphologies as their feature sizes are larger than our simulation box in many cases. We instead focus on swelling in the nanostructured part of the ternary phase diagram, that is, the lamellar and bicontinuous morphologies. When we fit our simulated domain spacings for $\varphi_{HP}<\varphi_{HP}^{**}$ to eq 3 and calculate $\beta(\alpha)$, we obtain the red squares shown in Figure 5. To ensure a more fair comparison between simulation and experiment then, we refit eq 3 to the experimental results through the bicontinuous microemulsions only. This refitting yields the gray circles reported in Figure 5.

The horizontal lines in Figure 5 denote the idealized "wet brush" (homopolymers mixed throughout BCP domains, β = 1/3) and "dry brush" (homopolymers localized in domain centers, β = 1) swelling regimes. Below α = 0.5, β increases with α toward the dry brush prediction (β = 1), supporting the idea that ternary blends show more dry brush character as homopolymer chain length increases. We note that all of the blends we studied showed β well above the wet brush model (β = 1/3), suggesting that blends must contain very short homopolymer chains ($\alpha < 0.2$) to exhibit complete miscibility of the block copolymers and homopolymers within the lamellae.

For $\alpha > 0.5$, the simulation results begin to deviate from eq 15 with simulation values of β flattening as α approaches unity. The refit experimental data show the same leveling off at β = 1 and a near-quantitative match with our simulations. This result should not be surprising since, according to the dry brush model, when β = 1, the HP are completely segregated in the center of the nanostructures, thus swelling lamellae only in the direction normal to the interface. A β value greater than 1 would indicate that the HP are not only completely segregated from the BCP, but are also stretching beyond their neat coiled dimensions in the blend. We conclude that, while β initially increases with α, it cannot increase significantly beyond the dry brush prediction in nanostructured blends. The apparent super swelling ($\beta \gg 1$) observed experimentally is actually an artifact of changes in the blend structural morphology following the bicontinuous microemulsion.

Finally, we investigate our simulation results for validation of the wet brush/dry brush mixing model between BCP brushes and HP monomers in lamellar domains. Figure 6 quantifies the distance of an individual monomer from the interface between the A and B domains. Given the difficulty of precisely defining the distance of a monomer from the interdomain interface for a given simulation snapshot, we approximate that value here by determining the shortest distance of a given monomer to the midpoint of the bond linking the A and B chains of any of the BCPs. The sharp BCP peak at low z represents the location of the interfacial A and B beads relative to the midpoint of the bond between them, which we find has an average length of ~0.9 DPD units. Thus, the distance z of the interfacial DPD beads to the defined interface should be ~0.45 DPD units on average, giving a very high probability that there will be a bead in the range $0.4 < z < 0.5$, followed by a low probability of DPD beads $0.5 < z < 0.6$ due to excluded volume effects from the interfacial beads. The broader peak located at higher z represents the distribution of beads partitioned toward the middle of the lamellae.

As we can see in Figure 6, the shorter HP chains (α = 0.2) penetrate more deeply into the BCP brushes than the longer HPs (α = 1.0). This dewetting of the brushes smoothly increases between α = 0.2 and α = 1.0 (results not shown). The boundary between the dewetted BCP/HP layers (α = 1.0) is not sharp as implied by eq 3 with $\beta \sim 1$, but exhibits some HP

penetration into the brush. We do observe that the longer HPs extend further from the A/B domain than the short HPs, indicative of increased swelling of the lamellar domain by the longer HPs. Thus, we conclude that despite the accuracy of eq 3 at describing the swelling of the mixture features, the exponent β does not fully capture the extent to which homopolymers wet/dewet the BCP brush layer; that is, even when $\beta = 1$, the homopolymers are not fully segregated from the BCP. As an aside, it is interesting to note that the brush monomer distributions are, to a first approximation, relatively insensitive to changes in wetting with increasing HP length. Nevertheless, we do observe the shoulder in the BCP monomer distribution near $z \sim 1.25$ extends slightly further from the A/B interface for the shorter HPs ($\alpha = 0.2$) than the longer HPs ($\alpha = 1.0$). This is indicative of weak swelling of the brush domain with decreasing HP length.

CONCLUSIONS

Comprehensive DPD simulations were performed to gain insights into the impact of adding homopolymers of varying lengths on the swelling and stability of symmetric ternary block copolymer-homopolymer blends (A_n-b-B_n/A_m/B_m). Our simulations reproduced the essential features of the experimental phase diagram, including: swelling of lamellar BCP domains with initial HP addition; formation of a bicontinuous microemulsion structure at a critical HP volume fraction φ^*_{HP}; and macrophase separation with ever increasing HP addition at $\varphi^{**}_{HP} > \varphi^*_{HP}$. DPD simulation predicted φ^*_{HP} as a function of α, the ratio of the HP to BCP chain lengths, more accurately than MFT, likely due to DPD's inclusion of thermal fluctuations that play a critical role in microemulsion formation. Our simulations also accurately predicted the extent of lamellar swelling with HP addition and changes in α. Specifically, we observed variations in the mechanism of domain swelling from wetting of the BCP brushes for shorter HPs ($\alpha < 0.5$) to nearly complete brush dewetting for even longer HPs, in excellent agreement with experimental observations. Our simulations, in turn, allowed us to observe the progressive dewetting of the BCP brushes by HPs of increasing length at a fixed φ_{HP}. Although theory (eqs 1 and 2) would suggest that the exponent (β) of the empirical model for domain swelling (eq 3) could be interpreted as a descriptor of HP/BCP segregation, our simulations find that the HPs and BCP brushes never completely segregate even for $\beta = 1$ (eq 2). Instead, HPs of increasing length progressively withdraw from the BCP layer to the domain centers, but always exhibit some brush overlap. For $\alpha > 0.5$, β plateaus at a value slightly higher than the theoretically predicted $\beta = 1$ (eq 2), suggesting that perhaps BCP and/or HP chains are slightly stretched in these blends. However, analyses of radius of gyration and bond lengths from DPD simulations (data not shown) did not provide evidence of such chain stretching, so we conclude that within simulation and experimental uncertainty, our results do not deviate significantly from theory. Thus, β provides an excellent quantitative prediction for domain swelling and a qualitative indicator of wetting/dewetting, but it does not accurately represent the extent of segregation between the HPs and BCPs. The results presented here are important to the fundamental understanding of BCP-HP blend behavior and the use of HP blending to tune nano and microstructure size and morphology. This work also demonstrates the value of DPD simulations for studying block copolymer blends.

ACKNOWLEDGMENTS

The authors gratefully acknowledge the support from the National Science Foundation through a Graduate Research Fellowship (A.D. Goodson, grant no. B55600G1), NSF-OIA no. 1430280, and DMR-1752611 (G. Liu). Additional support for this work came from the Louisiana Board of Regents (grant no. LEQSF(2015-18)-RD-A-18) and the Robert and Gayle Longmire Early Career Professorship in Chemical Engineering (J. N. L. Albert). The authors acknowledge Dr. Paul F. Nealey for insightful discussion and guidance on the experimental part of the work.

REFERENCES AND NOTES

1 F. S. Bates, *Science* **1991**, *251*, 898.

2 F. S. Bates, G. H. Fredrickson, *Annu. Rev. Phys. Chem.* **1990**, *41*, 525.

3 C. M. Bates, M. J. Maher, D. W. Janes, C. J. Ellison, C. G. Willson, *Macromolecules* **2013**, *47*, 2.

4 J. E. Poelma, K. Ono, D. Miyajima, T. Aida, K. Satoh, C. J. Hawker, *ACS Nano* **2012**, *6*, 10845.

5 M. P. Stoykovich, M. Müller, S. O. Kim, H. H. Solak, E. W. Edwards, J. J. De Pablo, P. F. Nealey, *Science* **2005**, *308*, 1442.

6 M. P. Stoykovich, E. W. Edwards, H. H. Solak, P. F. Nealey, *Phys. Rev. Lett.* **2006**, *97*, 147802.

7 R. J. Hickey, T. M. Gillard, M. T. Irwin, T. P. Lodge, F. S. Bates, *Soft Matter* **2016**, *12*, 53.

8 E. A. Jackson, M. A. Hillmyer, *ACS Nano* **2010**, *4*, 3548.

9 W. A. Phillip, B. O'Neill, M. Rodwogin, M. A. Hillmyer, E. L. Cussler, *ACS Appl. Mater. Interfaces* **2010**, *2*, 847.

10 R. M. Dorin, W. A. Phillip, H. Sai, J. Werner, M. Elimelech, U. Wiesner, *Polymer* **2014**, *55*, 347.

11 Y. Gu, U. Wiesner, *Macromolecules* **2015**, *48*, 6153.

12 Y. Zhang, N. E. Almodovar-Arbelo, J. L. Weidman, D. S. Corti, B. W. Boudouris, W. A. Phillip, *npj Clean Water* **2018**, *1*, 2.

13 T. H. Epps III , R. K. O'Reilly, *Chem. Sci.* **2016**, *7*, 1674.

14 Y. Xu, Y. Hoshi, C. K. Ober, *J. Mater. Chem.* **2011**, *21*, 13789.

15 G. Liu, M. P. Stoykovich, S. Ji, K. O. Stuen, G. S. Craig, P. F. Nealey, *Macromolecules* **2009**, *42*, 3063.

16 L. C. Messé, L. Corvazier, A. J. Ryan, *Polymer* **2003**, *44*, 7397.

17 K. A. Orso, P. F. Green, *Macromolecules* **1999**, *32*, 1087.

18 N. Torikai, N. Takabayashi, I. Noda, S. Koizumi, Y. Morii, Y. Matsushita, *Macromolecules* **1997**, *30*, 5698.

19 D. Q. Pike, M. Müller, J. J. de Pablo, *J. Chem. Phys.* **2011**, *135*, 114904.

20 G. S. Doerk, K. G. Yager, *ACS Nano* **2017**, *11*, 12326.

21 M. A. Hillmyer, W. W. Maurer, T. P. Lodge, F. S. Bates, K. Almdal, *J. Phys. Chem. B.* **1999**, *103*, 4814.

22 N. Zhou, T. P. Lodge, F. S. Bates, *J. Phys. Chem. B.* **2006**, *110*, 3979.

23 F. S. Bates, W. W. Maurer, P. M. Lipic, M. A. Hillmyer, K. Almdal, K. Mortensen, G. H. Fredrickson, T. P. Lodge, *Phys. Rev. Lett.* **1997**, *79*, 849.

24 H. Tanaka, T. Hashimoto, *Macromolecules* **1991**, *24*, 5713.

25 P. K. Janert, M. Schick, *Macromolecules* **1997**, *30*, 137.

26 H. Tanaka, H. Hasegawa, T. Hashimoto, *Macromolecules* **1991**, *24*, 240.

27 K. O. Stuen, C. S. Thomas, G. Liu, N. Ferrier, P. F. Nealey, *Macromolecules* **2009**, *42*, 5139.

28 M. F. Uddin, Z. Jiang, A. Raymond, A. D. Goodson, B. S. Lwoya, J. N. L. Albert, *J Polym Sci B* **2018**, *56*, 1443.

29 K. H. Dai, E. J. Kramer, K. R. Shull, *Macromolecules* **1992**, *25*, 220.

30 R. D. Groot, T. J. Madden, *J. Chem. Phys.* **1998**, *108*, 8713.

31 H.-J. Qian, Z.-Y. Lu, L.-J. Chen, Z.-S. Li, C.-C. Sun, *Macromolecules* **2005**, *38*, 1395.

32 A. A. Gavrilov, Y. V. Kudryavtsev, A. V. Chertovich, *J. Chem. Phys.* **2013**, *139*, 224901.

33 Z. Posel, M. Lísal, J. K. Brennan, *Fluid Phase Equilibria* **2009**, *283*, 38.

34 C. Soto-Figueroa, M.-d.-R. Rodríguez-Hidalgo, J.-M. Martínez-Magadán, L. Vicente, *Macromolecules* **2008**, *41*, 3297.

35 C. Soto-Figueroa, L. Vicente, J.-M. Martínez-Magadán, M.-d.-R. Rodríguez-Hidalgo, *Polymer* **2007**, *48*, 3902.

36 N. Chen, L.-T. Yan, X.-M. Xie, *Macromolecules* **2013**, *46*, 3544.

37 J. Noolandi, K. Hong, *Macromolecules* **1982**, *15*, 482.

38 D. Broseta, G. H. Fredrickson, *J. Chem. Phys.* **1990**, *93*, 2927.

39 R. J. Hickey, T. M. Gillard, M. T. Irwin, D. C. Morse, T. P. Lodge, F. S. Bates, *Macromolecules* **2016**, *49*, 7928.

40 P. K. Janert, M. Schick, *Macromolecules* **1997**, *30*, 3916.

41 J. Naughton, M. Matsen, *Macromolecules* **2002**, *35*, 8926.

42 Z. Bai, H. Guo, *Polymer* **2013**, *54*, 2146.

43 D. Düchs, V. Ganesan, G. H. Fredrickson, F. Schmid, *Macromolecules* **2003**, *36*, 9237.

44 R. K. Spencer, M. W. Matsen, *J. Chem. Phys.* **2018**, *148*, 204907.

45 M. Müller, M. Schick, *J. Chem. Phys.* **1996**, *105*, 8885.

46 S. Plimpton, *J. Comput. Phys.* **1995**, *117*, 1.

47 R. D. Groot, P. B. Warren, *J. Chem. Phys.* **1997**, *107*, 4423.

48 R. D. Groot, T. J. Madden, D. J. Tildesley, *J. Chem. Phys.* **1999**, *110*, 9739.

49 P. Nikunen, I. Vattulainen, M. Karttunen, *Phys Rev E* **2007**, *75*, 036713.

50 M. P. Allen, D. J. Tildesley, *Computer Simulation of Liquids*; Oxford University Press: New York, **1987**.

51 P. Espanol, P. Warren, *EPL (Europhys Lett)* **1995**, *30*, 191.

52 W. Humphrey, A. Dalke, K. Schulten, *J. Mol. Graph.* **1996**, *14*, 33.

53 S. Jury, P. Bladon, M. Cates, S. Krishna, M. Hagen, N. Ruddock, P. Warren, *Phys. Chem. Chem. Phys.* **1999**, *1*, 2051.

54 C. K. Knox, G. A. Voth, *J. Phys. Chem. B.* **2010**, *114*, 3205.

55 A. J. Ryan, S.-M. Mai, J. P. A. Fairclough, I. W. Hamley, C. Booth, *Phys. Chem. Chem. Phys.* **2001**, *3*, 2961.

56 Y. Li, H.-J. Qian, Z.-Y. Lu, *Polymer* **2013**, *54*, 3716.

57 F. S. Bates, W. Maurer, T. P. Lodge, M. F. Schulz, M. W. Matsen, K. Almdal, K. Mortensen, *Phys. Rev. Lett.* **1995**, *75*, 4429.